This CVPR2013 paper is the Open Access version, provided by the Computer Vision Foundation.
The authoritative version of this paper is available in IEEE Xplore.

Specular Reflection Separation using Dark Channel Prior

Hyeongwoo Kim
KAIST
hyeongwoo.kim@kaist.ac.kr

Hailin Jin
Adobe Research
hljin@adobe.com

Sunil Hadap
Adobe Research
hadap@adobe.com

Inso Kweon
KAIST
iskweon@kaist.ac.kr

Abstract

We present a novel method to separate specular reflection from a single image. Separating an image into diffuse and specular components is an ill-posed problem due to lack of observations. Existing methods rely on a specular-free image to detect and estimate specularity, which however may confuse diffuse pixels with the same hue but a different saturation value as specular pixels. Our method is based on a novel observation that for most natural images the dark channel can provide an approximate specular-free image. We also propose a maximum a posteriori formulation which robustly recovers the specular reflection and chromaticity despite of the hue-saturation ambiguity. We demonstrate the effectiveness of the proposed algorithm on real and synthetic examples. Experimental results show that our method significantly outperforms the state-of-the-art methods in separating specular reflection.

1. Introduction

The observed color of an image is formed from the spectral energy distributions of the light reflected by the surface reflectance, and the intensity of the color is determined by the imaging geometry. This imaging process can also be explained in terms of the diffuse and specular reflections according to their physical properties. Diffuse reflection can be assumed to be associated only with the relative angle between the light direction and the surface normal among the imaging geometry regardless of the viewing direction, while specular reflection is dependent on the viewing direction. As shown in Figure 1(a), natural objects tend to have the diffuse property as well as the specular property on the reflection model. However, the behavior of the specular reflection often leads to problems in many computer vision applications such as stereo matching, segmentation, and recognition. Most of the applications simply consider the observed image as a diffuse reflection model, regarding the specular reflection as outliers.

One of the notable works in separating specular reflection from a single image is studied by Tan and Ikeuchi [18].

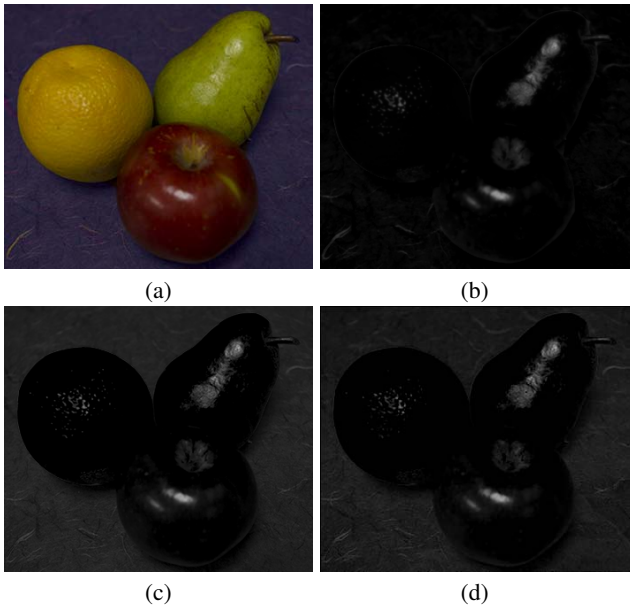

Figure 1. Specular separation. (a) Input image. (b) Our result. (c) Dark channel. (d) Result of [18]. Our result correctly distinguishes between diffuse and specular reflections, while the previous method inadequately recognizes the background region as specular reflection. Note that dark channel is similar to the specular component recovered by the previous method in many cases of natural images. Please refer to the electronic version for better visualization of all results in this paper.

Their method shows a satisfactory result, however it fails in the presence of the colors which have the same hue component with different saturation one. This hue-saturation ambiguity has been an issue in the recent studies of the single image-based specular reflection separation. To address the limit of the previous approaches, we introduce the statistics that a diffuse pixel of natural images in general has very low intensity in at least one color channel, motivated by the *dark channel prior* [4]. As shown in Figure 1(c), the dark channel of an image provides a pseudo specular reflection result, which is similar to the previous result shown in Figure 1(d). In this paper, we also propose a *maximum a posteriori* (MAP) approach that incorporates priors in the

reflection model, resulting in more stable separation of the specular reflection shown in Figure 1(b).

2. Related Work

Separating object reflectance into diffuse and specular components is one of the fundamental problems in the computer vision and graphics areas, which is made difficult by the subtle nature of the physics involved. Since the dichromatic reflection model [14] which represents the complex reflecting properties of a surface as a linear combination of the diffuse and specular components was introduced, this model has been adopted in modern approaches for color understanding. Based on the neutral interface reflection assumption [6, 3], the dichromatic model can be further simplified in a way that the spectral energy distribution of the specular component is approximated being identical to the one of incident light which is often regarded as pure white or estimated by [19].

To distinguish between diffuse and specular reflections from an observed image, most of approaches basically take into account the color information with the underlying dichromatic reflection model except for the hardware assisted method [20] which utilized a polarization reflectance model using Fresnel reflectance. Nayar *et al*. [12] improved this polarization-based method by incorporating color information that is the neighboring diffuse colors.

Some efforts have been made in separating the reflections with multiple images. Advantages of using the multi-view constraint come from the different physical properties of diffuse and specular reflections on the relation between lighting and viewing directions with respect to a surface normal. Sato and Ikeuchi [13] analyzed color signatures estimated from many images taken under a moving light source to compute specular reflection. Lin and Shum [9] took a couple of images with different light positions in order to obtain photometric images and estimate the intensities of the reflection components. The use of a pair of stereo images was also introduced by Lin *et al*. [8], where specular pixels are detected by color histogram and stereo correspondence is then employed to compute the corresponding diffuse components in other views. These approaches show satisfactory results in separating specular reflection, yet it is not always applicable in general cases due to the requirement of multiple images.

Besides the multiple images-based approaches, there have been a number of literatures separating the reflections from a single image. These approaches can be categorized in three ways. First, Klinker *et al*. [5] and Bajscy *et al*. [2] identified specular and diffuse reflections on the basis of color segmentation. As the second category, Tan *et al*. [16] successfully separated highlight reflections by using repeated textures. The third category is the analysis on different color spaces. Mallick *et al*. [11] proposed an SUV color space which is composed of S and UV channels representing specular and diffuse components respectively. They extended the use of this color space to highlight removal by eroding S channel in [10]. Tan *et al*. [18, 17] demonstrated the effective algorithm in the chromaticity intensity space, which exploits a pseudo specular-free image to detect the diffuse pixels and iteratively propagates the maximum chromaticity of the diffuse component to adjacent neighborhoods. This approach was improved by Yang *et al*. [22] who developed a fast bilateral filtering [21] approach for the purpose of refining maximum chromaticity with neighboring pixels in real-time.

In this paper, we present an approach that incorporates an effective pseudo specular-free image and priors for the separation of the specular reflection out of a single image. We show that the dark channel as an alternative pseudo specular-free image has merits against the previous one. In addition, our approach introduces priors on the specular reflection as well as the diffuse chromaticity in the dichromatic reflection model, whereas most of the previous methods only measure the fidelity to the reflection model. This naturally leads our formulation to a MAP problem.

3. Reflection Model

Dichromatic reflection model [14] has been widely used for understanding reflection properties of a scene taken by a color image. We model an image as a linear combination of diffuse and specular reflections according to the dichromatic model. Denoting the diffuse and specular reflections by $\mathbf{I}_d(\mathbf{x})$ and $\mathbf{I}_s(\mathbf{x})$ respectively, the observed image $\mathbf{I}(\mathbf{x})$ is simply expressed as:

$$\mathbf{I}(\mathbf{x}) = \mathbf{I}_d(\mathbf{x}) + \mathbf{I}_s(\mathbf{x}). \tag{1}$$

In our model, we represent the chromaticity of a color with the intensity normalized color vector:

$$\tilde{\mathbf{I}}(\mathbf{x}) = \frac{\mathbf{I}(\mathbf{x})}{\sum_{c\in\{r,g,b\}} I_c(\mathbf{x})}, \tag{2}$$

where $I_c(\mathbf{x})$ is one of the color channels. Let $\mathbf{\Lambda}(\mathbf{x})$ and $\mathbf{\Gamma}(\mathbf{x})$ represent the chromaticities of the diffuse and specular components respectively. Then Equation (1) can be equivalently written as:

$$\mathbf{I}(\mathbf{x}) = m_d(\mathbf{x})\mathbf{\Lambda}(\mathbf{x}) + m_s(\mathbf{x})\mathbf{\Gamma}(\mathbf{x}), \tag{3}$$

where m_d and m_s are the diffuse and specular reflection coefficients respectively, which depend on imaging geometry. We note that the diffuse chromaticity implies the inherent color of the surface while the specular chromaticity implies that of the illumination. Here, the specular chromaticity can be assumed to be uniform for a given image such that $\Gamma_r(\mathbf{x}) = \Gamma_g(\mathbf{x}) = \Gamma_b(\mathbf{x}) = 1/3$. Without loss

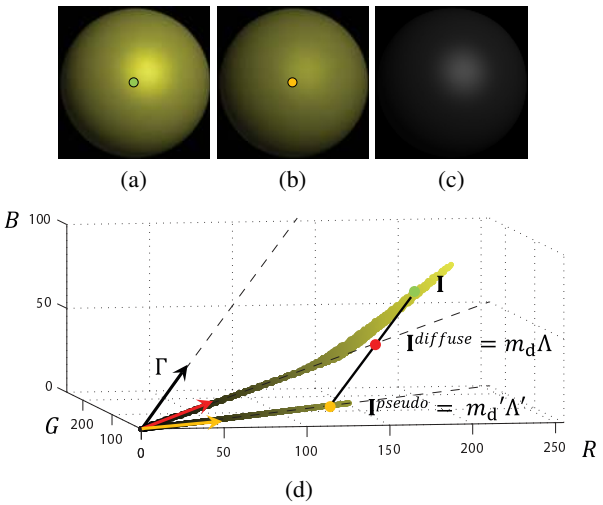

Figure 2. Geometric interpretation of our pseudo specular-free image and dark channel in the dichromatic reflection model. (a) Synthetic input image. (b) Pseudo specular-free image. (c) Dark channel. (d) Color distributions of (a) in the RGB space and (b) on the RG-plane.

of generality, this can be achieved by normalizing the illumination chromaticity estimated from [19] as preprocessing step.

Our goal is to estimate the specular reflection coefficient $m_s(\mathbf{x})$ from the observed single image $\mathbf{I}(\mathbf{x})$ so that the specular component $\mathbf{I}_s(\mathbf{x})$ can be recovered, multiplied by the uniform specular chromaticity $\mathbf{\Gamma}$, *i.e.*, $\mathbf{I}_s(\mathbf{x}) = m_s(\mathbf{x})\mathbf{\Gamma}$. In our formulation, we represent the dichromatic reflection model in the RG chromaticity space:

$$\tilde{\mathbf{I}}(\mathbf{x}) = \alpha(\mathbf{x})\mathbf{\Lambda}(\mathbf{x}) + (1 - \alpha(\mathbf{x}))\mathbf{\Gamma}, \tag{4}$$

where $\alpha = m_d/(m_d + m_s)$. Note that the specular reflection coefficient can be easily recovered from $m_s = (1-\alpha)(m_d+m_s)$, where $m_d+m_s = \sum_{c\in\{r,g,b\}}(m_d\Lambda_c + m_s\Gamma_c) = \sum_{c\in\{r,g,b\}} I_c$. Therefore, we have the likelihood of the specular reflection separation as:

$$E_D(\alpha, \mathbf{\Lambda}) = \sum_{\mathbf{x}} \left(\tilde{\mathbf{I}}(\mathbf{x}) - (\alpha(\mathbf{x})\mathbf{\Lambda}(\mathbf{x}) + (1 - \alpha(\mathbf{x}))\mathbf{\Gamma})\right)^2. \tag{5}$$

This data fidelity term is ill-posed with respect to α. The observed image only provides a partial constraint for the specular reflection coefficient as there are many counterparts of the diffuse reflection term resulting in the same observed image. This under-constrained problem can be resolved by specifying the diffuse chromaticity $\mathbf{\Lambda}$.

4. Dark Channel and Pseudo Specular-Free Image

To begin with, we shortly discuss typical algorithms and their limitations in determining the diffuse chromaticity $\mathbf{\Lambda}$.

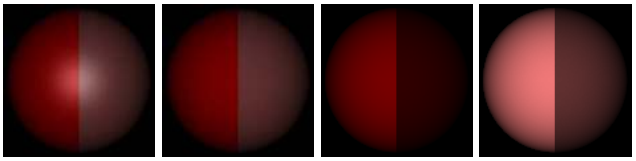

Figure 3. Comparison of pseudo specular-free images. (a) Input image. (b) Diffuse reflection of (a). (c) Our result. (d) Result of [18]. Our result is more closed to (b). In particular, the left parts of the hemispheres in (b) and (c) are identical.

Previous works [18, 22] utilize the pseudo specular-free image to detect the diffuse pixels and estimate the diffuse chromaticity, which is generated by shifting the maximum chromaticity of each pixel. However, these approaches are problematic especially when there exist pure diffuse reflections having the same hue but different saturation value since they are all detected as specular reflections.

To address this issue and improve the general performance, we introduce a simple but effective pseudo specular-free image followed by an efficient optimization framework. Motivated by [4], we exploits the dark channel to derive a new pseudo specular-free image. Based on our observation that a diffuse pixel is likely to have very low intensity in at least one color channel for most of natural images, we consider the dark channel as the rough estimate of the specular reflection for the input image. Thus, we obtain our pseudo specular-free image $\mathbf{I}^{pseudo}(\mathbf{x})$ by subtracting the dark channel $I^{dark}(\mathbf{x})$ from all color channels:

$$I_c^{pseudo}(\mathbf{x}) = I_c(\mathbf{x}) - I^{dark}, \tag{6}$$

$$I^{dark}(\mathbf{x}) = \min_{c\in\{r,g,b\}} I_c(\mathbf{x}). \tag{7}$$

Here, the dark channel is taken from the lowest intensity value among RGB channels at each pixel. As illustrated in Figure 2(d), this process is equivalent to project each pixel of the input image to one of the RG-, RB-, and, GB-planes along the illumination direction. In particular, the pseudo specular-free pixel (yellow dot) is obtained by projecting the pixel (green dot) of the input image to RG-plane along the illumination direction $\mathbf{\Gamma}$. We note that this pseudo specular-free pixel has the incorrect diffuse coefficient m_d' and chromaticity $\mathbf{\Lambda}'$ compared to the correct diffuse reflection component (red dot). We take the pseudo specular-free image and dark channel as the initial estimates of the diffuse and specular reflections respectively and then find the correct one by the optimization which will be explained later in detail.

This scheme has a couple of benefits against the previous approach [18]. As shown in Figure 3, our pseudo specular-free image provides the direct estimate for the diffuse reflection. For instance, the left parts of the hemispheres in Figure 3 (b) and (c) are shown to be exactly identical to each

Figure 4. Examples of dark channel. Top row shows real images and bottom one indicates the corresponding dark channels. The dark channels of the left half images are almost equivalent to the true specular reflection, while it fails for the right half ones due to saturation bias.

other. This is because the dark channel becomes close to the correct specular reflection as the diffuse reflection of an object has very low value in the saturation component as shown in Figure 4(a). It is notable that the specular separation results of the state-of-the-art algorithms [18, 22] are found to be similar to the dark channel of the input image in the most of our experiments (Figure 1(c) and (d)).

Following the algorithm of He *et al.* [4], the soft matting [7] can be examined to refine the dark channel as shown in Figure 5. The red arrow shown in Figure 5(a) indicates the strong specular reflection. We can see that the initial estimate of the specular reflection detected by the dark channel is undesirably propagated to neighborhoods as shown in Figure 5(c). This result reveals that refining the dark channel with the matting Laplacian [7] is not suitable for the specular separation and a different strategy is hence required.

5. Priors

In the following section, we present priors on the specular reflection as well as the diffuse chromaticity in the dichromatic in order to disambiguate meaningless solutions in Equation (5).

5.1. Smooth Variation of Specular Reflection

As shown in Figure 6(b), the gradient of the specular reflection tends to be smooth. This smoothness term has shown to produce stable estimates on the highlight removal in [15]. We define this smoothness prior as the isotropic TV-l_2 regulariser in terms of α:

$$E_S(\alpha) = \sum_{\mathbf{x}} \|\nabla(1-\alpha(\mathbf{x}))\|_2, \tag{8}$$

where ∇ is the gradient operator. Note that α is directly related to the specular coefficient m_s as discussed in Section 3.

(a) (b) (c)

Figure 5. (a) Input image. (b) Dark channel of (a). (c) Refinement of (b) using [4].

5.2. Locally Constant and Edge-Preserving Properties of Diffuse Chromaticity

We also introduce a prior to favor the physical properties of the diffuse chromaticity. By definition, the shading effect of the diffuse reflection disappears in the corresponding chromaticity due to the normalization (Equation (2)), leading interior homogeneity within each diffuse chromaticity region but sharp changes across them. Therefore, as shown in Figure 6(c), the correct diffuse chromaticity has a tendency to be constant over a local region and edge-preserving across the different chromaticities. We add an additional term to make the number of the diffuse chromaticities controlled, pursuing that the number of the specular- and shading-free diffuse chromaticities is limited in the general objects. For instance, the toy in Figure 6(c) approximately consists of 5 diffuse chromaticities. Consequently, the prior on the diffuse chromaticity is formulated as:

$$E_C(\mathbf{\Lambda}, \lambda) = \sum_{\mathbf{x}} \|\nabla \mathbf{\Lambda}_\lambda(\mathbf{x})\|_1 + \beta_\lambda \|\lambda(\mathbf{x})\|_0, \tag{9}$$

where $\tilde{\mathbf{\Lambda}}_\lambda(\mathbf{x})$ returns the chromaticity indicated by $\lambda(\mathbf{x})$ and $\lambda = \{1, \ldots, N\}$ denotes the index for a set of chromaticities. β_λ is the weight to balance the two terms. The first term is the typical TV-l_1 regulariser to encourage the locally constant and edge-preserving properties while the second one is l_0-norm to constrain the number of the diffuse chromaticities.

6. Optimization

As a general MAP optimization, our objective function is defined as a linear combination of the likelihood term and two prior terms:

$$E(\alpha, \mathbf{\Lambda}, \lambda) = E_D(\alpha, \mathbf{\Lambda}) + \beta_s E_S(\alpha) + \beta_c E_C(\mathbf{\Lambda}, \lambda), \tag{10}$$

where β_s and β_c are the regularization weights. While this objective function constrains the specular reflection and diffuse chromaticity in a robust manner, the discrete metric

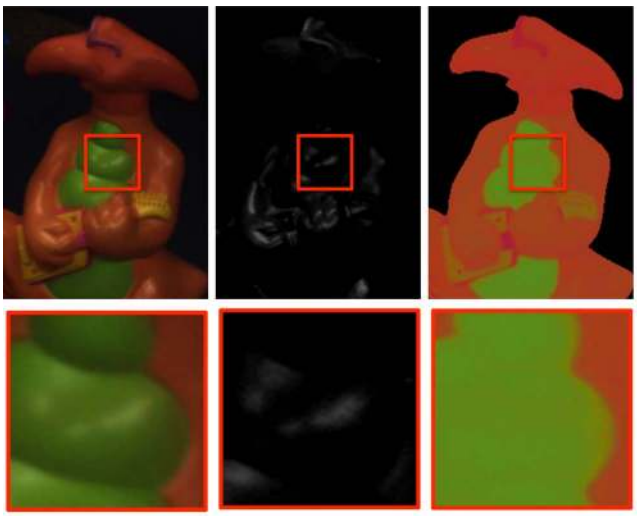

(a) (b) (c)

Figure 6. Priors in the dichromatic model. (a) Input image. (b) Specular reflection of (a). This indicates that the specular reflection tends to vary smoothly. The intensity of the result is scaled by a factor of 2 for a better visualization. (c) Diffuse chromaticity of (a). The diffuse chromaticity in general shows the locally constant and edge-preserving properties.

with l_0-norm in the energy term $E_C(\mathbf{\Lambda}, \lambda)$ makes the optimization computationally intractable. To minimize Equation (10) against the difficulty, we rewrite the smoothness term of the diffuse chromaticity and relax the objective function based on the quadratic relaxation [1], introducing the auxiliary variable $\tilde{\lambda}$ corresponding to λ:

$$E_C(\mathbf{\Lambda}, \lambda, \tilde{\lambda}) = \sum_{\mathbf{x}} \|\nabla \mathbf{\Lambda}_{\lambda}(\mathbf{x})\|_1 + \beta_{\lambda} \|\tilde{\lambda}(\mathbf{x})\|_0, \quad (11)$$

$$E(\alpha, \mathbf{\Lambda}, \lambda, \tilde{\lambda}) = E_D(\mathbf{\Lambda}, \alpha) + \beta_s E_S(\alpha) + \beta_c E_C(\mathbf{\Lambda}, \lambda, \tilde{\lambda}) + \frac{1}{2\theta}(\lambda - \tilde{\lambda})^2. \quad (12)$$

Here, θ controls the similarity between λ and $\tilde{\lambda}$. As $\theta \to 0$, this relaxed objective function is equivalent to Equation (10). Our overall algorithm is summarized in Algorithm 1. In the following section, we demonstrate an alternating minimization procedure to solve Equation (12).

6.1. Computing $\tilde{\lambda}$

For fixed α, $\mathbf{\Lambda}$, and λ, the objective function with respect to $\tilde{\lambda}$ can be written as:

$$\min_{\tilde{\lambda}} \left\{ \beta_{\tilde{\lambda}} \|\tilde{\lambda}(\mathbf{x})\|_0 + \frac{1}{2\theta}(\lambda(\mathbf{x}) - \tilde{\lambda}(\mathbf{x}))^2 \right\}, \quad (13)$$

where $\beta_{\tilde{\lambda}} = \beta_c \beta_{\lambda}$. It is a difficult problem due to the discrete nature of l_0-norm. To avoid the difficulty, we approximately minimize this energy by incorporating a progressive k-means clustering as shown in Figure 7(b). The solution $\tilde{\lambda}$ is simply taken as cluster indices. We first calculate a large number of clusters from the chromaticity image of our pseudo specular-free image, and then merge them progressively by measuring the distance of the chromaticities between each cluster. In this manner, we can obtain the solution of $\tilde{\lambda}$ efficiently.

Algorithm 1 Specular separation from a single image

Compute dark channel I^{dark} from the input image $\mathbf{I}$.
Compute pseudo specular-free image $\mathbf{I}^{pseudo}$ and its chromaticity $\tilde{\mathbf{I}}^{pseudo}$.
Compute k-means clustering on $\tilde{\mathbf{I}}^{pseudo}$.
Initialize λ^0 with the cluster indices and $\mathbf{\Lambda}^0$ with the cluster means and α^0 by solving Equation (5).
repeat
1: Solve $\tilde{\lambda}^{t+1}$ in Equation (13) for fixed α^t, $\mathbf{\Lambda}^t$, and λ^t.
2: Solve λ^{t+1} in Equation (14) for fixed α^t, $\mathbf{\Lambda}^t$, and $\tilde{\lambda}^t$.
3: Solve α^{t+1}, $\mathbf{\Lambda}^{t+1}$ in Equation (15) for fixed λ^t and $\tilde{\lambda}^t$.
until $E(\alpha^{t+1}, \mathbf{\Lambda}^{t+1}, \lambda^{t+1}, \tilde{\lambda}^{t+1}) - E(\alpha^t, \mathbf{\Lambda}^t, \tilde{\lambda}^t) < \kappa$.

6.2. Computing λ

For fixed α, $\mathbf{\Lambda}$, and $\tilde{\lambda}$, the objective function with respect to λ can be expressed as:

$$\min_{\lambda} \left\{ \beta_c \sum_{\mathbf{x}} \|\nabla \mathbf{\Lambda}_{\lambda}(\mathbf{x})\|_1 + \frac{1}{2\theta}(\lambda(\mathbf{x}) - \tilde{\lambda}(\mathbf{x}))^2 \right\}. \quad (14)$$

Solving this energy still remains complex because λ indicates a indexing variable. We again compute an approximated solution for this energy term. Once Equation (13) is solved, the cluster indices $\tilde{\lambda}(\mathbf{x})$ can be found along with the corresponding cluster means $\mathbf{\Lambda}_{\tilde{\lambda}}$. We perform an edge-preserving filtering (Figure 7(c)) for the computed diffuse chromaticity $\mathbf{\Lambda}_{\tilde{\lambda}}$, and then assign new labels for each pixel $\lambda(\mathbf{x})$ by searching for the closest diffuse chromaticity among $\mathbf{\Lambda}_{\tilde{\lambda}}$.

It can be noticed that θ in Equation (12) is adapted to small value for the tight relaxation in iterations, configured as a large initial value which enables employing the separate clustering algorithm.

6.3. Computing α, $\mathbf{\Lambda}$

For fixed $\tilde{\lambda}$ and λ, the object function with respect to α and $\mathbf{\Lambda}$ can be represented as:

$$\min_{\alpha, \mathbf{\Lambda}} \left\{ \sum_{\mathbf{x}} \left(\tilde{\mathbf{I}}(\mathbf{x}) - (\alpha(\mathbf{x}) \mathbf{\Lambda}(\mathbf{x}) + (1 - \alpha(\mathbf{x})) \mathbf{\Gamma}) \right)^2 + \beta_s \sum_{\mathbf{x}} \|\nabla(1 - \alpha(\mathbf{x}))\|_2 + \beta_c \sum_{\mathbf{x}} \|\nabla \mathbf{\Lambda}_{\lambda}(\mathbf{x})\|_1 \right\}. \quad (15)$$

(a) (b) (c)

Figure 7. Optimization on the diffuse chromaticity. (a) Estimated diffuse reflection. (b) Clustering indices. (c) Edge-preserving filtering.

This energy function can be further decomposed into the subproblems minimizing the energy functional in the form of TV-l_2 with respect to α; and the other functional having the form of TV-l_1 with respect to $\mathbf{\Lambda}$. Because each split functional is convex, it can be efficiently minimized by solving the associated Lagrangians.

7. Experimental Results

To evaluate our algorithm, we tested our algorithm on a synthetic case for which ground truths of diffuse and specular reflections are given along with its chromaticities. Accordingly, quantitative validation is only made on the synthetic case. In addition, we conducted experiments on several natural images captured by a Canon EOS 7D camera with linear response function, where diffuse and specular reflections are estimated using previously developed methods [18, 22] for the comparison. β_s and β_c in Equation (10) are all set to 0.1 empirically. β_λ in Equation (11) is set to 0.3, however our algorithm is not sensitive to its choice. For the progressive k-means clustering in Equation (13), the initial number of clusters is set to $k = 100$. The initial clusters are set to the best solution among ten restarts.

7.1. Synthetic Analysis

Figure 8 shows results for a synthetic image, which is generated by a hemisphere rendered with the two colors. The color in the left half is red, RGB = (150, 0, 0), while the saturation value of this color is increased to 50% in the right half color, thus this image exhibits a color distribution which lies on the same plane in RGB color space. As shown in the bottom row, [18] inadequately propagates the maximum chromaticities of diffuse pixels to specular pixels across the texture boundary, regarding the difference in the saturation value as specular reflection. Due to the each prior in the proposed method, our result robustly separates the diffuse chromaticity (c) and specular reflection (d) much more than [18].

7.2. Real Images

We compare our method with the images provided by [18, 22] in Figure 9. These images have no hue-saturation ambiguity, therefore it qualatitvely shows a similar performance.

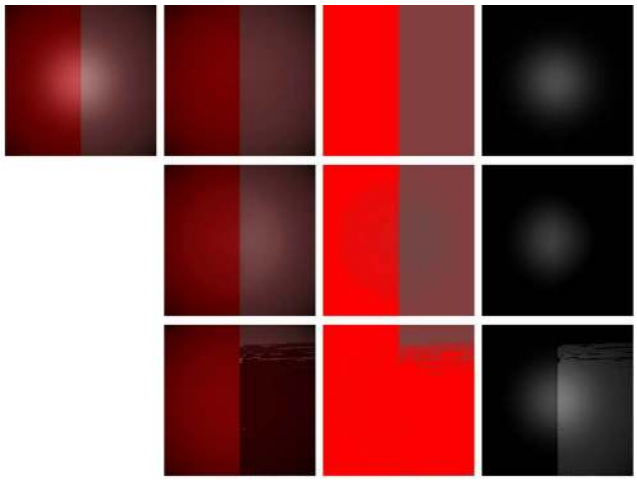

(a) (b) (c) (d)

Figure 8. Synthetic result. (a) Image generated by a hemisphere with same hue but different saturation colors. (b) Diffuse reflection. (c) Diffuse chromaticity. (d) Specular reflection. Top row: ground truth. Middle row: our result. Bottom row: result of [18].

Figure 10 shows the visual comparison for the real images, where our algorithm significantly improves the performance of the specular reflection separation. The failure of the previous methods shown in (d) and (e) comes from the incorrect detection of diffuse pixels. It is shown that the dark channels of these examples give the specular reflections which is similar with the result of the previous approache [18]. Our optimization framework further refines the dark channel in order to achieve more plausible diffuse and specular reflections as shown in (b) and (c) respectively, favoring the proposed priors.

We note that in the bottom row of Figure 10, the boundaries of the balloons are unexpectedly recognized as specular pixels. This mainly arises from the inaccurate clustering result of the diffuse chromaticity. For this reason, our algorithm can fail when facing mixed pixels around color boundaries and highly textured surfaces.

8. Conclusions

In this paper, we have presented a MAP optimization framework to separate specular reflection from a single image. Our method employes the dark channel as an initial estimate of specular reflection. The dark channel is found to be considerably identical to the specular reflection result of the previous approach. The optimization framework also includes priors to favor the smooth variation of specular component as well as the locally constant and edge-preserving properties of diffuse chromaticity. Our method is evaluated on both synthetic and real images to convince the

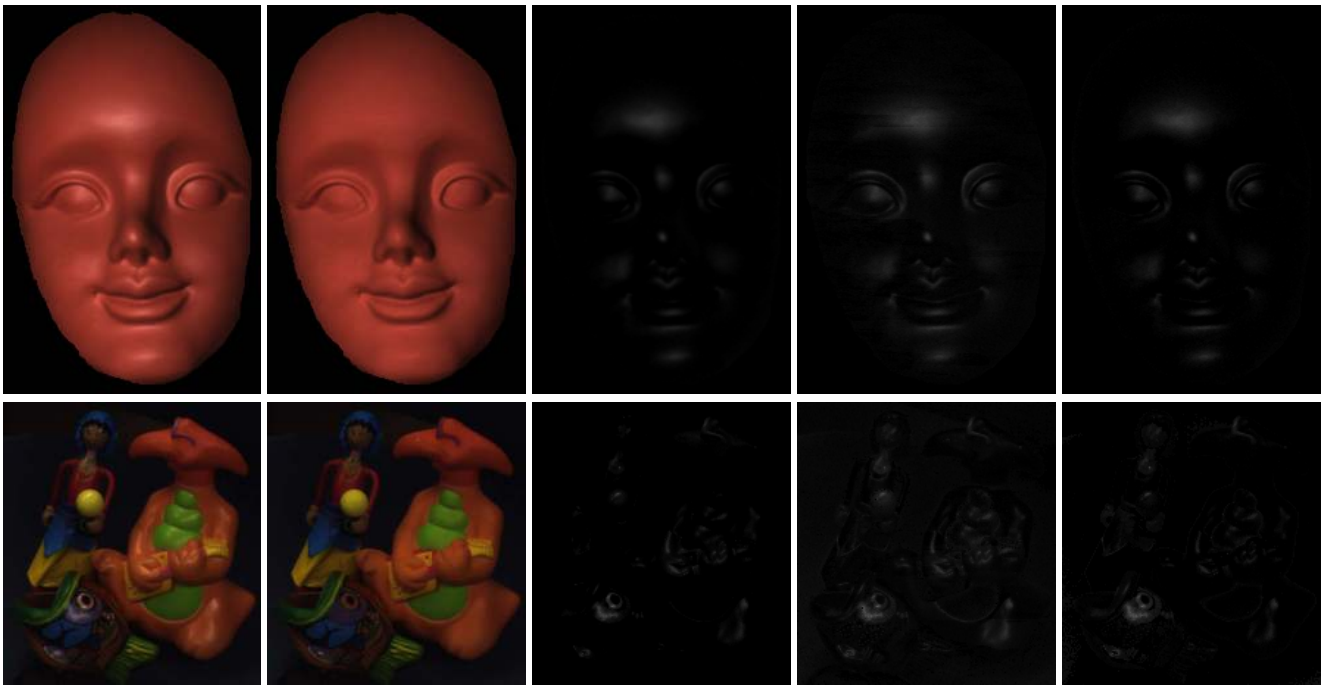

(a) (b) (c) (d) (e)

Figure 9. Qualitative comparison. (a) Input image. (b) and (c) Diffuse and specular reflections of our result. (d) Result of [18]. (e) Result of [22].

performance. The proposed method achieves more robust results in the presence of two distinct diffuse colors having the same hue but different saturation value, and qualitatively outperforms the state-of-the-art methods for most of natural images.

As discussed in the real examples, color boundaries are unfortunately found as specular pixels in some results. In the future work, we plan to reduce this artifact by improving the robustness of the clustering algorithm for the noise and highly textured surfaces.

9. Acknowledgements

This work is supported in part by Adobe System Incorporated and National Research Foundation of Korea 2012-0000986.

References

[1] J.-F. Aujol, G. Gilboa, T. F. Chan, and S. Osher. Structure-texture image decomposition - modeling, algorithms, and parameter selection. *IJCV*, 67(1):111–136, 2006.

[2] R. Bajcsy, S. W. Lee, and A. Leonardis. Detection of diffuse and specular interface reflections and inter-reflections by color image segmentation. *IJCV*, 17(3):241–272, 1996.

[3] G. D. Finlayson and G. Schaefer. Solving for colour constancy using a constrained dichromatic reflection model. *IJCV*, 42(3):127–144, 2001.

[4] K. He, J. Sun, and X. Tang. Single image haze removal using dark channel prior. *PAMI*, 33(12):2341–2353, 2011.

[5] G. J. Klinker, S. A. Shafer, and T. Kanade. The measurement of highlights in color images. *IJCV*, 2(1):7–32, 1988.

[6] H.-C. Lee, E. J. Breneman, and C. P. Schulte. Modeling light reflection for computer color vision. *PAMI*, 12(4):402–409, 1990.

[7] A. Levin, D. Lischinski, and Y. Weiss. A closed-form solution to natural image matting. *PAMI*, 30(2):228–242, 2008.

[8] S. Lin, Y. Li, S. B. Kang, X. Tong, and H.-Y. Shum. Diffuse-specular separation and depth recovery from image sequences. In *ECCV*, 2002.

[9] S. Lin and H.-Y. Shum. Separation of diffuse and specular reflection in color images. In *CVPR*, 2001.

[10] S. P. Mallick, T. Zickler, P. N. Belhumeur, and D. J. Kriegman. Specularity removal in images and videos: A PDE approach. In *ECCV*, 2006.

[11] S. P. Mallick, T. Zickler, D. J. Kriegman, and P. N. Belhumeur. Beyond Lambert: reconstructing specular surfaces using color. In *CVPR*, 2005.

[12] S. K. Nayar, X.-S. Fang, and T. Boult. Separation of reflection components using color and polarization. *IJCV*, 21(3):163–186, 1997.

[13] Y. Sato and K. Ikeuchi. Temporal-color space analysis of reflection. *JOSA*, 11(11):2990–3002, 1994.

[14] S. A. Shafer. Using color to separate reflection components. *Color Res. Appl.*, 10(4):210–218, 1985.

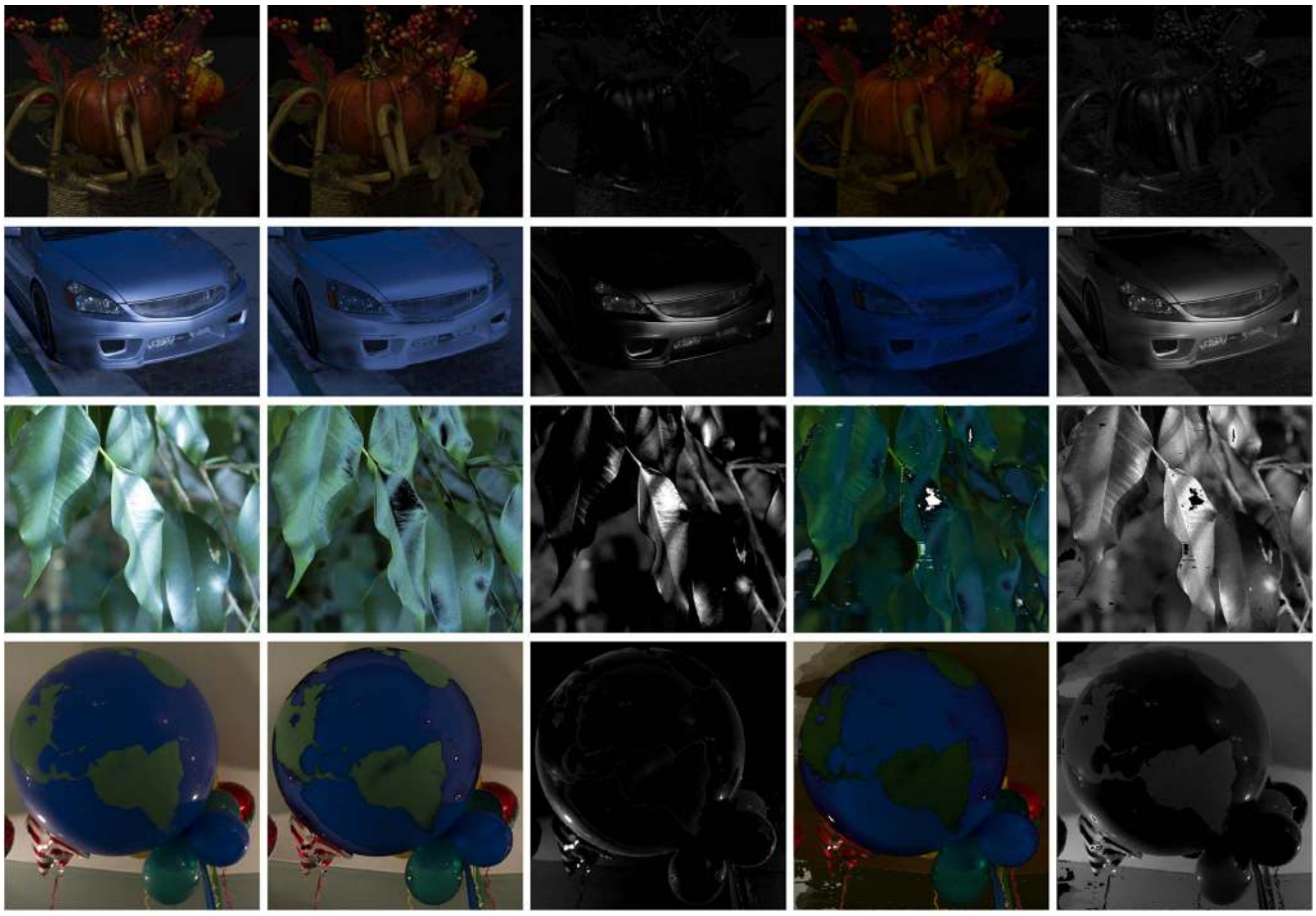

(a) (b) (c) (d) (e)

Figure 10. Natural images. (a) Input image. (b) and (c) Diffuse and specular reflections of our result. (d) and (e) Diffuse and specular reflections of [18].

[15] P. Tan, S. Lin, L. Quan, and H.-Y. Shum. Highlight removal by illumination-constrained inpainting. In *ICCV*, 2003.

[16] P. Tan, L. Quan, and S. Lin. Separation of highlight reflections on textured surfaces. In *CVPR*, 2006.

[17] R. T. Tan and K. Ikeuchi. Reflection components decomposition of textured surfaces using linear basis functions. In *CVPR*, 2005.

[18] R. T. Tan and K. Ikeuchi. Separating reflection components of textured surfaces using a single image. *PAMI*, 27(2):178–193, 2005.

[19] R. T. Tan, K. Nishino, and K. Ikeuchi. Illumination chromaticity estimation using inverse-intensity chromaticity space. In *CVPR*, 2003.

[20] L. B. Wolff and T. E. Boult. Constraining object features using a polarization reflectance model. *PAMI*, 13(7):635–657, 1991.

[21] Q. Yang, K.-H. Tan, and N. Ahuja. Real-time O(1) bilateral filtering. In *CVPR*, 2009.

[22] Q. Yang, S. Wang, and N. Ahuja. Real-time sepcualr highlight removal using bilateral filtering. In *ECCV*, 2010.